Anomalous helimagnetic domain shrinkage due to the weakening of the Dzyaloshinskii-Moriya interaction in CrAs

B. Y. Pan [1,2] H. C. Xu [1] Y. Liu,[3] R. Sutarto,[4] F. He,[4] Y. Shen,[1] Y. Q. Hao,[1] J. Zhao,[1] Leland Harriger [5] and D. L. Feng[1,6,7,*]

[1]*State Key Laboratory of Surface Physics, Department of Physics, and Advanced Materials Laboratory, Fudan University, Shanghai 200433, China*
[2]*School of Physics and Optoelectronic Engineering, Ludong University, Yantai, Shandong 264025, China*
[3]*Center for Correlated Matter, Zhejiang University, Hangzhou 310058, China*
[4]*Canadian Light Source, Saskatoon, Saskatchewan, Canada S7N 2V3*
[5]*NIST Center for Neutron Research, National Institute of Standards and Technology, 100 Bureau Drive, Gaithersburg, Maryland 20899, USA*
[6]*Collaborative Innovation Center of Advanced Microstructures, Nanjing 210093, China*
[7]*Hefei National Laboratory for Physical Science at Microscale and Department of Physics, University of Science and Technology of China, Hefei, Anhui 230026, China*

CrAs is a well-known helimagnet with the double-helix structure originating from the competition between the Dzyaloshinskii-Moriya interaction (DMI) and antiferromagnetic exchange interaction J. By resonant soft-x-ray scattering, we observe the magnetic peak $(0\ 0\ q_m)$ that emerges at the helical transition with $T_S \approx 267.5$ K. Intriguingly, the helimagnetic domains significantly shrink on cooling below ~ 255 K, opposite to the conventional thermal effect. The weakening of DMI on cooling is found to play a critical role here. It causes the helical wave vector to vary, ordered spins to rotate, and extra helimagnetic domain boundaries to form at local defects, thus leading to the anomalous shrinkage of helimagnetic domains. Our results indicate that the size of magnetic helical domains can be controlled by tuning DMI in certain helimagnets.

I. INTRODUCTION

In correlated materials, multiple magnetic interactions, including the superexchange, the Dzyaloshinskii-Moriya interaction (DMI), Kondo coupling, and the Ruderman-Kittel-Kasuya-Yosida interaction, may coexist, and they favor different ground states. The competition between these magnetic interactions leads to rich and novel phenomena, such as the quantum criticality in a Kondo lattice [1], spin liquid states in frustrated systems [2], and the emergence of magnetic skyrmions in helimagnets [3,4]. Tuning the strength of these interactions would be an important way to engineer the magnetic quantum states and properties. Take a helimagnet system, for example. Its magnetic Hamiltonian can be generally written as

$$H = \sum_{i,j} \vec{D}_{ij} \cdot (\vec{S}_i \times \vec{S}_j) + J_{i,j}\vec{S}_i \cdot \vec{S}_j, \qquad (1)$$

in which $\vec{D}_{i,j}$ and $J_{i,j}$ denote the antisymmetric DMI and the symmetric exchange interactions between $\vec{S}_i$ and $\vec{S}_j$, respectively. By changing temperature, magnetic field, material thickness, or pressure, the system can be continuously tuned into helical, conical, Skyrme crystal, or other quantum phases depending on the subtle balance of DMI, J, Zeeman coupling, and thermal fluctuations [5–8]. In particular, the nanosized

helimagnetic domains, a key ingredient for spintronics [9], can be delicately manipulated by external fields. For example, *in situ* Lorentz microscopy of $Fe_{0.5}Co_{0.5}Si$ film showed that a magnetic field can effectively deform, rotate, and enlarge the helimagnetic domains by applying H along different directions [10]. A similar observation was recently reported in Te-doped Cu_2OSeO_3 [11]. Here, in the helimagnet CrAs, we observe an anomalous shrinkage of helimagnetic domains with decreasing temperature, and we find the decrease of DMI in CrAs on cooling as its main driving force. This effect is contrary to conventional thermal behavior, and it may be harnessed for domain engineering in spintronics.

The helical transition temperature of CrAs is $T_S = 265$ K, and its spin helix propagates along the c axis [Fig. 2(a)] [5,12,13]. The local space-inversion symmetry breaking at the Cr and As sites gives rise to DMI, which is essential in stabilizing the double-helix spin structure as revealed by the group-theoretical approach [14]. Compared with other helimagnets in the MnP-type structure, such as MnP and FeP, the DMI in CrAs is much more pronounced [14,15]. In addition, recent studies show that CrAs exhibits novel non-Fermi-liquid behavior, unconventional superconductivity, and quantum criticality under certain conditions [13,16–20], and the helical magnetism is believed to be crucial in these fascinating properties [21]. The strong DMI and rich quantum phases in CrAs make it an exciting playground to study the behavior of magnetic domains under the competition between DMI and J.

---
*dlfeng@fudan.edu.cn

In our experiment, we used soft-x-ray absorption and resonant scattering to study the helical magnetism of CrAs. The magnetic resonant peak $(0\,0\,q_m)$ was observed at the chromium L-edge. Thanks to the high momentum resolution of the resonant soft-x-ray scattering (RSXS) technique, we could reveal the average helimagnetic domain size ξ and its temperature-dependent evolution. Intriguingly, unlike conventional magnets whose magnetic domains always grow larger on cooling, the domain size of CrAs substantially *decreases* with lowering temperature below $\sim$255 K. The average domain size in the ac plane shrinks by $\sim$44.14% from 255 to 20 K. We find that the temperature-dependent domain shrinkage follows the weakening of DMI, whose competition with J varies the helimagnetic wave vector. As the helical magnetic chains propagate across the crystal defects with decreasing DMI on cooling, extra helix domain boundaries form and the average domain size decreases, leading to the observed domain shrinkage opposite to the conventional thermal effect.

II. EXPERIMENT

CrAs single crystals were grown by the Sn-flux method described in a previous report [23]. The obtained shiny crystals have a needlelike shape with a typical size of $6 \times 1 \times 0.5$ mm^3. The largest crystalline plane is $(0\,0\,1)$. Electronic resistivity from 300 to 2 K was characterized by the Physical Properties Measurement System (PPMS). RSXS and x-ray absorption (XAS) experiments on a CrAs single crystal were performed using a four-circle diffractometer at the Resonant Elastic and Inelastic X-ray Scattering (REIXS) beamline of Canadian Light Source (CLS). The REIXS beamline is equipped with Elliptical Polarized Undulators (EPU) and can provide both σ- and π-polarized incident photons. For the RSXS signal, a silicon photodiode was used, while the XAS in total electron yield (TEY) mode and total fluorescence yield (TFY) mode were collected using a drain current and microchannel plate (MCP) detector, respectively. Single-crystal neutron diffraction (ND) was measured at the SPINS cold triple-axis spectrometer of the NIST Center for Neutron Research.

III. RESULTS AND DISCUSSION

The resistivity of experimental crystal shows a transition into the helical magnetic phase at 263 K [Fig. 1(a)], in agreement with previous reports [23]. Figure 1(b) is the XAS of CrAs (red line) measured by TEY at the Cr L-edge. To elucidate the Cr valance state, the XAS of Cr$_2$O$_3$ and CrO$_2$ were plotted together as the fingerprint of Cr^{3+} and Cr^{4+} valence states [22], respectively. The bulk sensitive TFY spectrum of CrAs was simultaneously collected. Both the TEY and TFY spectra of CrAs are consistent with the typical Cr^{3+} spectrum. These results show that the sample surface is clean and the valance state is Cr^{3+} with the $3d^3$ electronic configuration. Theoretically, the spin-only magnetic moment of Cr^{3+} is $3.87\mu_B$ [24], however the observed value is $1.7\mu_B$ [25]. The reduction of a magnetic moment in CrAs should come from fluctuations and the hybridization effect, similar to the case in MnP [26].
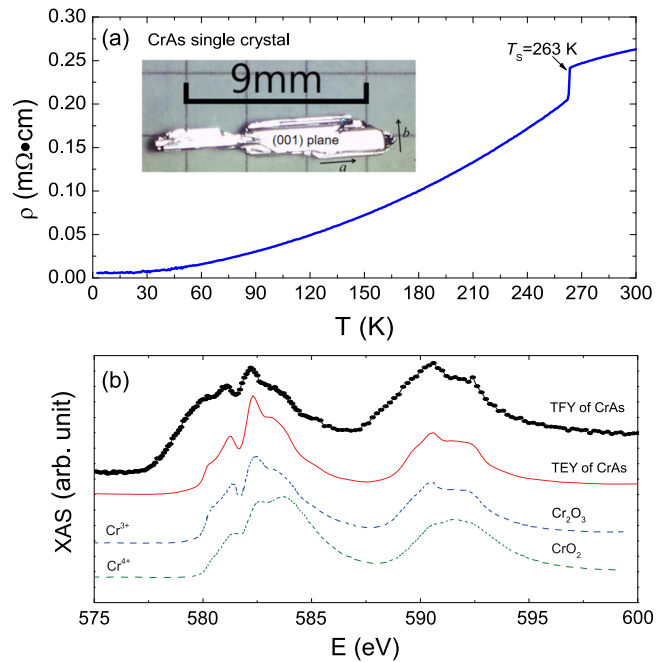

FIG. 1. (a) Resistivity of CrAs single crystal. The helical transition appears at $T_S = 263$ K. The inset panel shows the CrAs crystal with a needlelike shape. (b) X-ray absorption spectroscopy (XAS) in total electron yield (TEY) mode of CrAs at the Cr L-edge (red solid line), in comparison with two reference compounds Cr$_2$O$_3$ (blue dashed line) and CrO$_2$ (olive dashed line) from the literature [22]. The bulk sensitive total fluorescence yield (TFY) spectra of CrAs (black dots) was simultaneously collected.

In our RSXS experiment, the scattering crystalline plane is ac and the momentum transfer direction is along $(0\,0\,L)$ [Fig. 2(a)]. In this configuration, the electric field of horizontally (vertically) polarized incident photons is perpendicular (parallel) to the b axis. In the helical state below T_S, the Cr^{3+} spin moments lie in the ab easy plane, and the magnetic propagation wave vector is about $(0\,0\,0.356)$ at $T = 4$ K [13]. From sample alignment, we determined that the lattice constants are $a = 5.412(9)$ Å, $b = 3.348(1)$ Å, and $c = 6.007(9)$ Å at 20 K. Figure 2(b) presents the L scans around the magnetic wave vector $k_m = (0\,0\,q_m)$ with the resonant ($E = 578.7$ eV, π polarization) and nonresonant ($E = 570$ eV, π polarization) energies at $T = 20$ K. A strong resonant peak appears around $(0\,0\,0.352)$, consistent with the previously reported helical propagation wave vector [25].

To verify the magnetic nature of the $(0\,0\,q_m)$ peak, we measured its resonant profiles as a function of x-ray energy and wave vector $(0\,0\,L)$ at $T = 20$ K (Fig. 3). The incident x-ray is either vertically [σ, Fig. 3(a)] or horizontally [π, Fig. 3(b)] polarized. No distinction was made on the polarization of scattered photons, so the detected scattering intensities in our experiment are $I_\pi = I_{\pi\pi'} + I_{\pi\sigma'}$ and $I_\sigma = I_{\sigma\pi'} + I_{\sigma\sigma'}$. The observed results show that I_π is about 1.7 times stronger than I_σ. We further integrate the resonant intensity in Figs. 3(a) and 3(b) along the L direction, and we get the q-integrated intensities I_σ^{int} and I_π^{int}, as shown in Fig. 3(c). The line-shape profiles of I_σ^{int} (black line) and I_π^{int} (red line) are similar, except the latter is apparently stronger. The polarization dependence
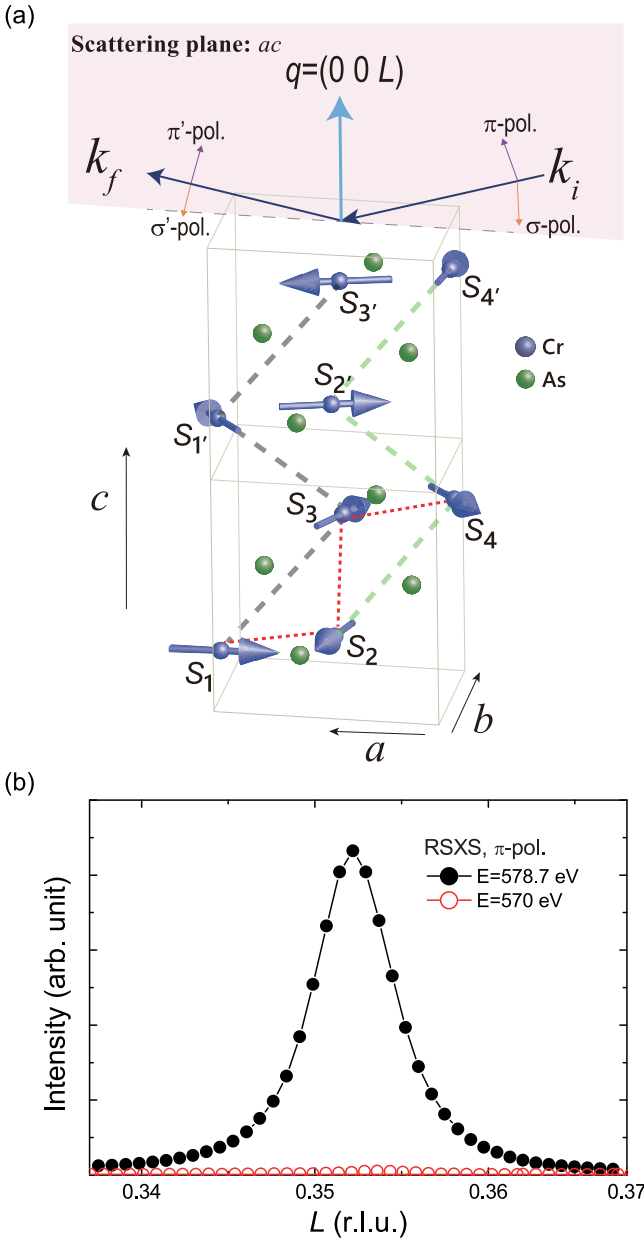
FIG. 2. (a) Illustration of the helical spin order in CrAs and the RSXS scattering geometry. The gray and green dashed lines denote the double spin helix chains running along the c axis. The red dashed lines denote the nearest-neighboring spins in a unit cell. (b) L scans of the $(0\,0\,q_m)$ magnetic peak with the resonant energy $E = 578.7$ eV (black dots) and nonresonant energy $E = 570$ eV (red circles) at $T = 20$ K. The incident photons are π-polarized.

of resonant profiles is consistent with magnetic scattering from a helimagnet, as evidenced by the following theoretical analysis. The scattering intensity from a helimagnet can be expressed as $I_{\mathrm{mag}} = |f_{\mathrm{mag}}|^2$, and $|f_{\mathrm{mag}}|$ is the resonant magnetic scattering length [27–29]:

$$
\begin{aligned}
f_{\mathrm{mag}} &= \begin{pmatrix} f_{\sigma\sigma'} & f_{\pi\sigma'} \\ f_{\sigma\pi'} & f_{\pi\pi'} \end{pmatrix} \\
&= -iF^1 \begin{pmatrix} 0 & M_a\cos\theta + M_c\sin\theta \\ M_c\sin\theta - M_a\cos\theta & -M_b\sin2\theta \end{pmatrix},
\end{aligned} \quad (2)
$$

where σ' and π' denote the polarization of outgoing photons; θ is the angle between the incident x-ray and the sample surface; and M_a, M_b, and M_c are the spin moment along the three crystal axes. In our case, $M_a = M_b$, $M_c = 0$, so $|f_{\sigma\pi'}| = |f_{\pi\sigma'}|$, $I_\sigma = I_{\sigma\pi'} = I_{\pi\sigma'}$. In this way, $I_\pi = I_{\sigma\pi'} + I_{\pi\pi'} > I_\sigma$, so I_π is always stronger than I_σ within the Cr L-edge resonant energy range; this is consistent with the experiment observation shown in Fig. 3.

We have also performed ND experiment on CrAs single crystal for a comparative study with RSXS. The L scans of the $(0\,0\,q_m)$ peak at various temperatures by RSXS ($E = 578.7$ eV, π-polarization) and ND are shown in Figs. 4(a) and 4(b), respectively. The RSXS and ND data agree with each other on the temperature dependence of peak intensity [Fig. 4(c)] and q_m [Fig. 4(d)]. The change of q_m with decreasing temperature indicates that the balance of competition between different magnetic interactions in CrAs varies with temperature. As can be seen in Fig. 4(e), the full width at half-maximum (FWHM) of ND diffractions is about seven times broader than that of RSXS, reflecting the higher instrumental resolution of RSXS. Actually, the instrumental resolution of RSXS in our experiment (<0.0008 Å^{-1} at the Cr L-edge) is much smaller than the measured resonance peak width, which is 0.0056 Å^{-1} at 20 K. So RSXS can directly probe the intrinsic magnetic peak width of CrAs and provide information on the magnetic domains.

Figure 5 shows scans of the $(0\,0\,q_m)$ resonance peak in reciprocal space at various temperatures by RSXS ($E = 578.7$ eV, π-polarization). The L and H scans have different profile shapes, and they can be empirically fitted by the Gauss and Lorentz functions, respectively [Figs. 5(a) and 5(b)]. As the profile of the magnetic resonance peak is mainly determined by the sample, the different profile shapes in L and H scans indicate distinguished domain distributions along the c and a axes. This anisotropy may come from the unique propagating direction of the helimagnetic wave vector or the elongated needlelike crystal shape, both of which are along the c axis and could cause anisotropic grain and strain distribution inside the sample.

The temperature-dependent evolutions of peak intensity, propagation wave vector q_m, and the average helimagnetic domain size ξ ($\xi = 1/\mathrm{FWHM}$ [30]) in L and H scans are presented in Figs. 5(c) and 5(d). Here, we directly used the original data in Figs. 5(a) and 5(b) for analysis and did not deconvolve the instrumental resolution due to its relatively small value. In Fig. 5(c), the magnetic peak intensity rapidly saturates below T_S, consistent with the first-order transition character [13]. The average helimagnetic domain sizes ξ_c and ξ_a rapidly grow from T_S to 255 K [Fig. 5(d)], consistent with the typical critical behavior near a transition point [31]. However, below ~255 K both ξ_c and ξ_a abnormally *decrease* on cooling [Fig. 5(d)]. The broadening of the magnetic peak also leads to a slight decreasing of peak intensity along H [Fig. 5(c)]. Usually, the average helimagnetic domain size of a magnetic order should monotonically increase below T_S because thermal fluctuations are weakened and spins become more correlated on cooling. The anomalous ξ versus T in CrAs indicates that the average helimagnetic domain size actually shrinks with lowering temperature.
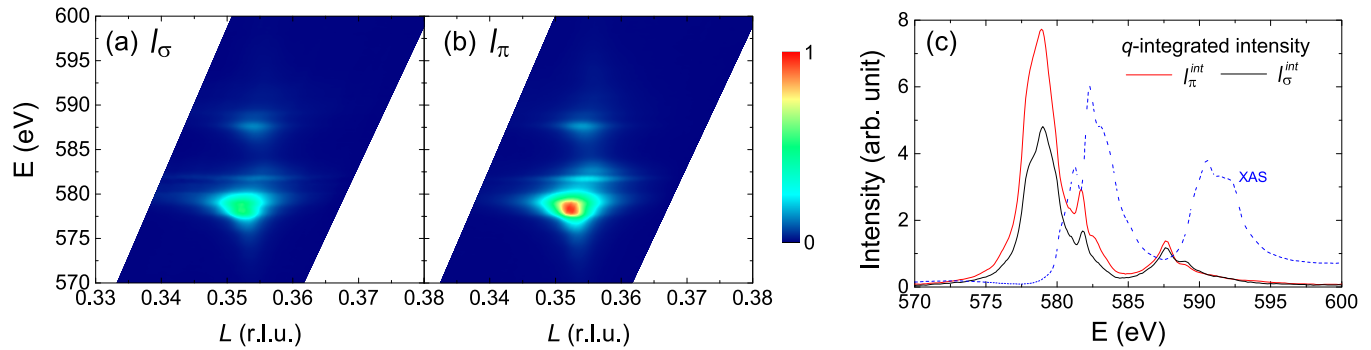
FIG. 3. Resonant profiles around (0 0 q_m) with (a) σ- or (b) π-polarized incident photons at $T = 20$ K. The resonance profiles are plotted as a function of photon energy covering the Cr L-edge and reciprocal lattice (0 0 L). All data were measured by a photodiode detector, and the fluorescence background has been subtracted. The color bar indicates scattering intensity in arbitrary units. (c) Integrated intensity along the L direction of the resonances in (a,b) as a function of the incident photon energy. The black and red lines represent the σ- and π-polarized incident photons, respectively. The dashed blue line is the XAS curve.

To reveal the possible thermal history effect, the sample was first cooled down from above T_S to 20 K (step 1), and then warmed up back to above T_S (step 2). The overall temperature-dependent evolution of peak intensity and ξ_c during steps 1 and 2 shows little thermal history effect, as shown in Fig. 6. However, there is a hysteresis between the cooling and warming curves around T_S [inset of Fig. 6(a)], consistent with the feature of first-order magnetic transition in CrAs [23].

The anomalous shrinkage of magnetic domains on cooling can be interpreted by the weakening of DMI in CrAs. In Ref. [13], the authors gave a detailed description of the magnetic interactions in CrAs. Its magnetic Hamiltonian was represented by Eq. (1), in which $\vec{D}_{i,j}$ and $J_{i,j}$ are the DMI and antiferromagnetic interactions between the nearest neighbors, respectively. The nearest-neighboring spins in a single unit

cell are illustrated by the red dashed lines in Fig. 2(a). q_m can be expressed as [13]

$$q_m = \frac{\beta_{12} + \beta_{23}}{\pi}, \qquad (3)$$

where β_{12} is the angle between $\vec{S}_1$ and $\vec{S}_2$, and β_{23} is the angle between $\vec{S}_2$ and $\vec{S}_3$. In the temperature range of our study, β_{23} barely changes [13]. Therefore, the decrease of q_m on cooling is mainly attributed to the variation of β_{12}, which is
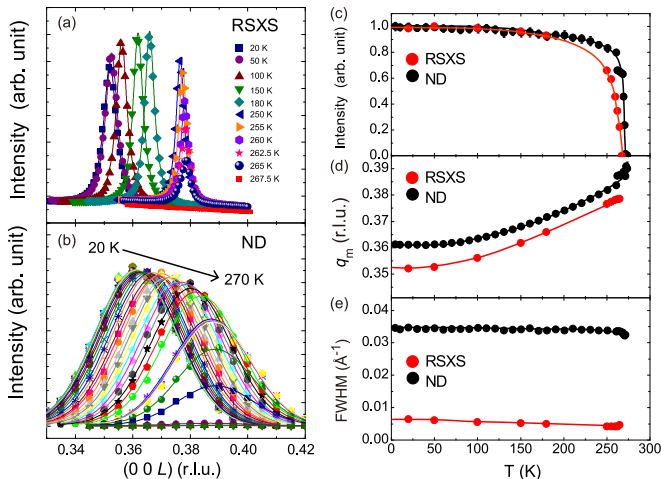

FIG. 4. Temperature dependence of the magnetic peak in CrAs single crystals probed by (a) RSXS and (b) ND in the warming process. The temperature range is from 20 to 270 K. The neutron diffraction peaks are much broader than the ones from RSXS. Comparison of the (c) intensity, (d) propagation wave vector, and (e) FWHM of a magnetic peak measured by RSXS (red dots) and neutron diffraction (black dots) as a function of temperature. The solid lines are guides to the eye.
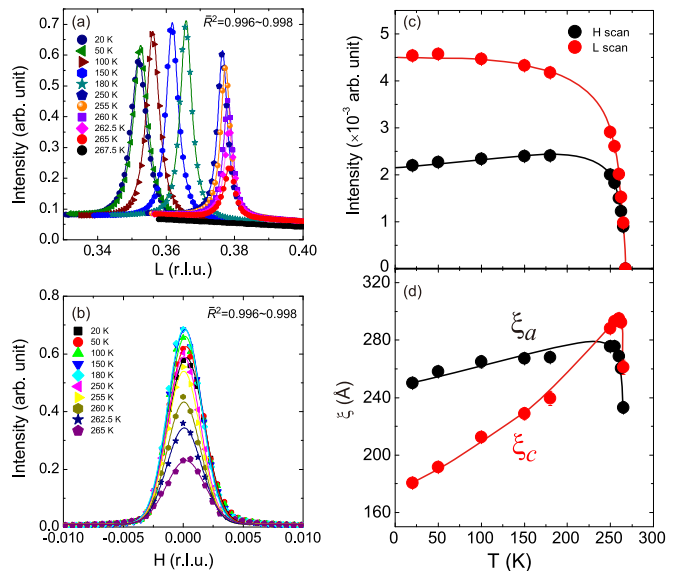

FIG. 5. Temperature-dependent evolution of the (0 0 q_m) resonant peak along (a) L and (b) H directions in the temperature range from 267.5 to 20 K. The incident photon energy is 578.7 eV with π polarization. The sample was warmed up from 20 to 267.5 K. The solid lines in (a) and (b) are Lorentz and Gauss function fittings, respectively. The adjusted R-square $\bar{R}^2$ of these fittings ($\bar{R}^2 > 0.994$) are shown in the panels. (c) Integrated intensity of the resonant peak and (d) the average helimagnetic domain size ξ vs temperature for the L (red dots) and H (black dots) scans. The solid lines are guides to the eye.
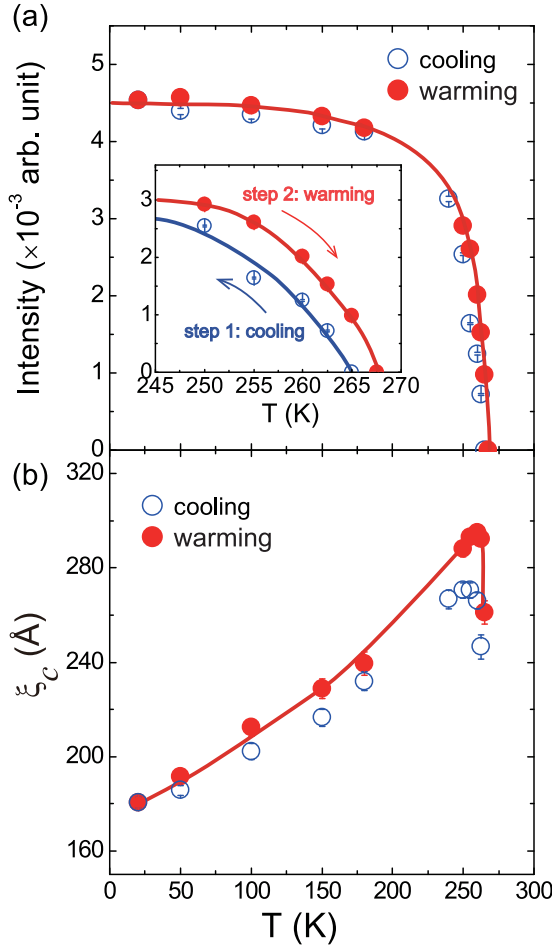
FIG. 6. Temperature dependence of (a) resonant peak intensity and (b) correlation length ξ_c in the cooling (step 1, blue circles) and warming (step 2, red dots) sequences. The inset of (a) shows the hysteresis between cooling and warm-up curves around T_S. The solid lines are guides to the eye.

determined by

$$\beta_{12} = \mathrm{tg}^{-1}(D_{12}^c/J_{12}), \tag{4}$$

in which D_{12}^c is the $\vec{D}_{12}$ component along the c axis. There are antiferromagnetic interactions between all nearest spins. In contrast, DMI exists between $\vec{S}_1$ and $\vec{S}_2$ but is absent between $\vec{S}_2$ and $\vec{S}_3$ [13]. Moreover, the DMI in CrAs is exceptionally larger than the antiferromagnetic interaction ($|D| > |J|$) [14]. Therefore, the induced change of β_{12} and the decreasing of q_m should be dominated by the variation of D_{12}^c:

$$\Delta(q_m) \propto \Delta(D_{12}^c). \tag{5}$$

According to this equation, the 6.70% decrease of propagation wave vector, from $q_m = 0.3773(5)$ at 255 K to $q_m = 0.3520(6)$ at 20 K, indicates that D_{12}^c become weaker. Since D_{12}^c favors noncollinear spin alignment and J_{12} favors antiparallel spin alignment in CrAs [13], $\vec{S}_1$ and $\vec{S}_2$ tend to be more antiparallel [13], as illustrated by β_{12} in Fig. 7. This again evidences the weakening of DMI with decreasing temperature. As DMI is the dominant force determining the spin
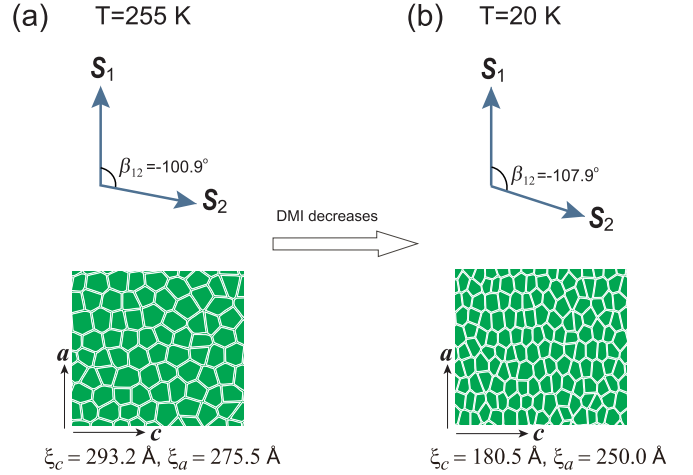

FIG. 7. Cartoon illustration of the angle (β_{12}) between $\vec{S}_1$ and $\vec{S}_2$ and helimagnetic domains in the ac plane at (a) 255 K and (b) 20 K. The values of β_{12} are from Ref. [13]. As the DMI term in the magnetic Hamiltonian has the form $\vec{D}_{12} \cdot (\vec{S}_1 \times \vec{S}_2)$, thus $\vec{D}_{12}$ favors noncollinear spin alignment. The tendency to antiferromagnetic spin alignment between $\vec{S}_1$ and $\vec{S}_2$ from 255 to 20 K indicates that the DMI gets weaker on cooling.

rotation along the helix chain, its weakening will make the helimagnetic domains easier to break up at the defect sites. As q_m varies with temperature, the neighboring spins continuously modulate their relative spin angles on cooling, which would generate additional domain boundaries at defect sites given the weakening DMI, in other words, the helimagnetic domains shrink. A straightforward cartoon illustration for the DMI controlled spin angle β_{12} and the accompanied domain shrinkage is presented in Fig. 7.

The helimagnetic domain shrinkage is anisotropic and mainly takes place along the c direction. As shown in Fig. 5(d), from 255 to 20 K the percentage drops of ξ_c and ξ_a are 38.44% and 9.26%, respectively. Here we define the spatial anisotropic ratio of domain shrinkage as $\gamma_{ca} = \frac{\Delta\xi_c/\xi_c(255\ \mathrm{K})}{\Delta\xi_a/\xi_a(255\ \mathrm{K})} = 4.15$. This is consistent with the fact that the helimagnetic order is propagating along the c direction. Meanwhile, it is intriguing to note that the DMI of CrAs is $\vec{D}_{12} \approx D_0(-0.17, -0.5, 0.85)$ [13], so the ratio of DMI components along c and a is $\kappa_{ca} = |D_{12}^c/D_{12}^a| = 5$. The similar size of γ_{ca} and κ_{ca} implies a possible role played by DMI in the anisotropy of domain shrinkage, as certain interactions exist in a and b directions as well.

By contrast, in our previous RSXS investigation on MnP, which is a helimagnet similar to CrAs in lattice and magnetic structures but whose propagation wave vector increases on cooling [5], the domain shrinkage behavior was not observed [26]. This implies that the decrease of q_m or DMI on cooling is the key to the formation of new domain boundaries at defect sites inside the sample. It should be noted that in most 3d-transition metal pnictides, the strength of DMI is much smaller than J, however CrAs is an exception in which $|D| > |J|$ [14]. The strong DMI of CrAs even drives the spin reorientation transition and the decrease of the magnetic wave vector under pressure [13]. Therefore, we conclude that the pronounced DMI strength combined with its decrease

on cooling are essential ingredients for the anomalous helimagnetic domain shrinkage behavior in CrAs. Broadening of a magnetic peak at low temperature was also observed in $Ca_3Co_2O_6$ with ferromagnetic chains, while it is attributed to the development of a short-range order [32], which is distinct from the single-component magnetic peak in CrAs and does not involve DMI.

IV. CONCLUSION

In summary, we find the Cr^{3+} valence state in CrAs, and our RSXS experiment reveals that its helimagnetic domains shrink on cooling below ~ 255 K. The domain shrinkage has a similar temperature-dependent evolution to that of DMI, indicating DMI is the main driving force in this anomalous behavior. Our results reveal a quantum effect that is contrary to the conventional thermal effect, and they suggest that DMI may be tuned to manipulate the domain boundaries in helimagnets, which may have application in future spintronics.

[1] H. v. Löhneysen, A. Rosch, M. Vojta, and P. Wölfle, Rev. Mod. Phys. **79**, 1015 (2007).

[2] C. Broholm, R. J. Cava, S. A. Kivelson, D. G. Nocera, M. R. Norman, and T. Senthil, Science **367**, eaay0668 (2020).

[3] U. K. Rößler, A. N. Bogdanov, and C. Pfleiderer, Nature (London) **442**, 797 (2006).

[4] J. H. Han, J. Zang, Z. Yang, J.-H. Park, and N. Nagaosa, Phys. Rev. B **82**, 094429 (2010).

[5] K. Motizuki, H. Ido, T. Itoh, and M. Morifuji, *Electronic Structure and Magnetism of 3d-Transition Metal Pnictides* (Springer, Berlin, Heidelberg, 2010).

[6] S. Mühlbauer, B. Binz, F. Jonietz, C. Pfleiderer, A. Rosch, A. Neubauer, R. Georgii, and P. Böni, Science **323**, 915 (2009).

[7] C. Dhital, L. DeBeer-Schmitt, Q. Zhang, W. Xie, D. P. Young, and J. F. DiTusa, Phys. Rev. B **96**, 214425 (2017).

[8] A. Chacon, A. Bauer, T. Adams, F. Rucker, G. Brandl, R. Georgii, M. Garst, and C. Pfleiderer, Phys. Rev. Lett. **115**, 267202 (2015).

[9] P. Schoenherr, J. Müller, L. Köhler, A. Rosch, N. Kanazawa, Y. Tokura, M. Garst, and D. Meier, Nat. Phys. **14**, 465 (2018).

[10] M. Uchida, Y. Onose, Y. Matsui, and Y. Tokura, Science **311**, 359 (2006).

[11] M.-G. Han, J. A. Garlow, Y. Kharkov, L. Camacho, R. Rov, J. Sauceda, G. Vats, K. Kisslinger, T. Kato, O. Sushkov, Y. Zhu, C. Ulrich, T. Söhnel, and J. Seidel, Sci. Adv. **6**, eaax2138 (2020).

[12] H. Boller and A. Kallel, Solid State Commun. **9**, 1699 (1971).

[13] Y. Shen, Q. Wang, Y. Hao, B. Pan, Y. Feng, Q. Huang, L. W. Harriger, J. B. Leao, Y. Zhao, R. M. Chisnell, J. W. Lynn, H. Cao, J. Hu, and J. Zhao, Phys. Rev. B **93**, 060503(R) (2016).

[14] A. Kallel, H. Boller, and E. F. Bertaut, J. Phys. Chem. Solids **35**, 1139 (1974).

[15] J. Sjostrom, J. Phys.: Condens. Matter **4**, 5723 (1992).

[16] W. Wu, J. Cheng, K. Matsubayashi, P. Kong, F. Lin, C. Jin, N. Wang, Y. Uwatoko, and J. Luo, Nat. Commun. **5**, 5508 (2014).

[17] M. Matsuda, F. K. Lin, R. Yu, J.-G. Cheng, W. Wu, J. P. Sun, J. H. Zhang, P. J. Sun, K. Matsubayashi, T. Miyake, T. Kato, J.-Q. Yan, M. B. Stone, Q. Si, J. L. Luo,, and Y. Uwatoko, Phys. Rev. X **8**, 031017 (2018).

[18] H. Kotegawa, S. Nakahara, R. Akamatsu, H. Tou, H. Sugawara, and H. Harima, Phys. Rev. Lett. **114**, 117002 (2015).

[19] C. Y. Guo, M. Smidman, B. Shen, W. Wu, F. K. Lin, X. L. Han, Y. Chen, F. Wu, Y. F. Wang, W. B. Jiang, X. Lu, J. P. Hu, J. L. Luo, and H. Q. Yuan, Phys. Rev. B **98**, 024520 (2018).

[20] S. Park, S. Shin, S.-I. Kim, S. Kim, C.-K. Park, J. D. Thompson, and T. Park, npj Quantum Mater. **4**, 49 (2019).

[21] M. R. Norman, Physics **8**, 24 (2015).

[22] Y. S. Dedkov, A. S. Vinogradov, M. Fonin, C. Konig, D. V. Vyalikh, A. B. Preobrajenski, S. A. Krasnikov, E. Y. Kleimenov, M. A. Nesterov, U. Rudiger, S. L. Molodtsov, and G. Guntherodt, Phys. Rev. B **72**, 060401(R) (2005).

[23] W. Wu, X. D. Zhang, Z. H. Yin, P. Zheng, N. L. Wang, and J. Luo, Sci. China **53**, 1207 (2010).

[24] H. P. Meyers, *Introductory Solid State Physics* (CRC, Boca Raton, FL, 1997).

[25] K. Selte, A. Kjekshus, W. E. Jamison, A. F. Andresen, and J. E. Engebretsen, Acta Chem. Scand. **25**, 1703 (1971).

[26] B. Y. Pan, H. Jang, J.-S. Lee, R. Sutarto, F. He, J. F. Zeng, Y. Liu, X. W. Zhang, Y. Feng, Y. Q. Hao, J. Zhao, H. C. Xu, Z. H. Chen, J. P. Hu, and D. L. Feng, Phys. Rev. X **9**, 021055 (2019).

[27] H. Jang, B. Y. Kang, B. K. Cho, M. Hashimoto, D. Lu, C. A. Burns, C.-C. Kao, and J.-S. Lee, Phys. Rev. Lett. **117**, 216404 (2016).

[28] S. W. Lovesey and S. P. Collins, *X-Ray Scattering and Absorption by Magnetic Materials* (Clarendon, Oxford, 1996).

[29] M. Ramakrishnan, Y. Joly, Y. W. Windsor, L. Rettig, A. Alberca, E. M. Bothschafter, P. Lejay, R. Ballou, V. Simonet, V. Scagnoli, and U. Staub, Phys. Rev. B **95**, 205145 (2017).

[30] G. Helgesen, J. P. Hill, T. R. Thurston, D. Gibbs, J. Kwo, and M. Hong, Phys. Rev. B **50**, 2990 (1994).

[31] M. Janoschek, M. Garst, A. Bauer, P. Krautscheid, R. Georgii, P. Böni, and C. Pfleiderer, Phys. Rev. B **87**, 134407 (2013).

[32] S. Agrestini, L. C. Chapon, A. Daoud-Aladine, J. Schefer, A. Gukasov, C. Mazzoli, M. R. Lees, and O. A. Petrenko, Phys. Rev. Lett. **101**, 097207 (2008).